Modeling DC Motor Drive Systems in Power System Dynamic Studies

Shengqiang Li, *Member, IEEE*, Xiaodong Liang, *Senior Member, IEEE*, and Wilsun Xu, *Fellow, IEEE*

***Abstract*—Direct current (dc) motor drive systems are extensively used in paper, steel, mining, material handling, and other industrial applications due to the high starting torque and easy speed control over a wide range. They could account for 10%–20% load demand in some industrial facilities and thus have significant impact on the overall system dynamics. However, an adequate dynamic model for this type of loads is not available for power system dynamic studies. In this paper, a comprehensive modeling method for dc motor drive systems is proposed considering two scenarios: 1) The drive will trip when subjected to severe voltage sags, and 2) the drive can ride through when experiencing mild voltage sags. The dc drive trip curve and a simple procedure to determine if the drive needs to be included for dynamic studies are proposed for Scenario 1. The dynamic model for dc motor drive systems, which can be readily inserted in the simulation software, is developed and verified through case studies for Scenario 2.**

***Index Terms*—DC drive trip curve, dc drives, dynamic model, power system dynamic studies, transfer functions, voltage sags.**

NOMENCLATURE

Parameters:

R_d	Direct current (dc) armature circuit resistance (total).
L_d	dc armature circuit inductance (total).
K_{pc}	Proportional constant of proportional–integral (PI) current controller.
K_{ic}	Integral constant of PI current controller.
K_{ps}	Proportional constant of PI speed controller.
K_{is}	Integral constant of PI speed controller.
λ	Overloading factor of the dc drive.
K_E	Voltage constant of the dc motor.
K_T	Torque constant of the dc motor.
J	Moment of inertia of the dc motor.
L_C	Commutating inductance.

Variables:

V	Utility-side bus voltage, per-unit.
V_0	Initial value of utility-side bus voltage, per-unit (prefault).
$V_{\lg}$	Alternating current (ac) voltage of the rectifier, phase-to-ground.
$V_{\lg 0}$	Initial value of ac voltage of the rectifier, phase-to-ground (prefault).
$I_{\rm ac}$	AC-side phase current (rms).
P	Active power of the load.
P_0	Initial value of active power of the load (prefault).
Q	Reactive power of the load.
Q_0	Initial value of reactive power of the load (prefault).
S	Apparent power consumption of the drive.
S_0	Initial value of apparent power consumption of the drive (prefault).
P_n	Rated motor horsepower.
I_n	Nominal dc motor armature current.
ω_n	Nominal dc motor speed.
$I_{\rm dc}$	Averaged dc motor armature current.
$V_{\rm dc}$	Averaged output voltage of silicon-controlled rectifier (SCR)-bridge converter.
E_g	Averaged motor-generated voltage [back electromotive force (EMF)].
α	Firing angle of SCR-bridge converter.

Manuscript received December 30, 2013; revised June 16, 2014; accepted July 2, 2014. Date of publication July 8, 2014; date of current version January 16, 2015. Paper 2013-PSEC-1012.R1, presented at the 2014 IEEE/IAS Industrial and Commercial Power Systems Technical Conference, Fort Worth, TX, USA, May 20–23, and approved for publication in the IEEE TRANSACTIONS ON INDUSTRY APPLICATIONS by the Power Systems Engineering Committee of the IEEE Industry Applications Society.

S. Li is with the Power System Studies Group, Powertech Labs Inc., Surrey, BC V3W 3J4, Canada (e-mail: sli.zju@gmail.com).

X. Liang is with Electrical Engineering, School of Engineering and Computer Science, Washington State University, Vancouver, WA 98686-9600 USA (e-mail: xiaodong.liang@wsu.edu).

W. Xu is with the Department of Electrical and Computer Engineering, University of Alberta, Edmonton, AB T6G 2R3, Canada (e-mail: wxu@ualberta.ca)

Color versions of one or more of the figures in this paper are available online at http://ieeexplore.ieee.org.

Digital Object Identifier 10.1109/TIA.2014.2336972

I. INTRODUCTION

THE dc motors can provide a high starting torque, offer easy speed control over a wide range, and thus find their extensive usage in paper, steel, mining, material handling, and other industrial applications. The dc drives have been used for many decades to control the speed and torque of dc motors. The speed control methods of a dc motor are simpler and less expensive than those of ac motors, and the speed control over a large range both below and above rated speed can be easily achieved [1], [2]. Usually, the dc motor drive system consists of a three-phase rectifier, the dc motor, and the control system [2], [3].

DC drives account for 10%–20% of power demand in some industrial facilities. For example, dc drives consume 17.6% of the total load demand and are supplied through dedicated transformers in a 22-MW paper mill facility [4]. Therefore, dc motor drive systems could have significant impact on the overall system dynamics. As a common type of load in industrial facilities, dc motor drive systems (sometimes in large scale) need to be modeled adequately in power system dynamic studies; however, the reality is that their dynamic model is currently not available.

The IEEE Task Force on Load Representation for Dynamic Performance [5] recommends that an adjust speed drive (ASD) is an effectively constant power load if it is able to ride through voltage sags without tripping. It is recommended that ASDs are like computers and electronic equipment, except that shutdown will typically occur when the voltage drops below the lowest tolerance, about 90% of normal. Response to voltage is fast relative to rotor angle oscillations, so such loads are effectively constant power even in first-swing and small-signal stability studies, so long as voltage is above the point at which shutdown occurs. DC motor drive systems are one type of ASDs. However, as indicated in [6], using a constant power load to represent such a complex nonlinear power electronics component is questionable; a more accurate dynamic modeling method for dc motor drive systems is required for power system dynamic studies.

Traditionally, the modeling of a dc motor drive system has been well established in the field of control engineering. In [7], a state space model designed for the permanent magnet dc motor drive with proportional-integral-derivative controllers is presented. A discrete-time model for dc motor drive system is proposed in [8]. Since these models are designed primarily for tuning control parameters, the system voltage is treated as a constant parameter rather than a variable. However, when the modeling power system loads, the system voltage should always be explicitly expressed as an input variable. Therefore, the models proposed in [7] and [8] are not suitable for power system dynamic studies.

Due to the lack of proper dynamic models, dc drives are treated simply as transparent devices for the dynamic performance simulation in commercial simulation software such as ETAP [9]. In ETAP, "transparent devices" means the load that is tripped during the fault period and recovers to the initial power consumption immediately after the fault clears [9]. DC drives are complex nonlinear power electronics devices, but their modeling method in the simulation software is based on simplifications and no verification is done to show how far such simplifications will be introduced compared to the reality.

Over the recent years, power electronic device modeling was mostly focused on the averaged modeling of power electronics converters/rectifiers at the component level [10]–[12]. Switching power converters (SPCs) belong to a very special class of subjects to be controlled. Due to the switching action, which is common to every SPC, the converter's model switches periodically between a set of ordinary differential equations. The whole model is a differential equation system with discontinuous right-hand-side functions. Such systems will be simply termed as discontinuous systems. In the control literature, they are also called variable structure systems. One approach for controlling SPC is to transform the discontinuous system models into continuous ones so that control methods for continuous systems become applicable. Averaging methods are the means for achieving these objectives. With averaging methods, the discontinuity of the original discontinuous models is smoothed, and in many cases, the averaged models will be continuous [10]. The dynamic averaged-value model (AVM) of a three-phase load-commutated converter is proposed in [13]; however, such AVM is just at the converter level, and the dc motor and the control system are not considered. The literature survey shows that the AVM for a complete set of the dc motor drive system is currently unavailable.

How to create an adequate dynamic model of dc motor drive systems for power system dynamic studies is investigated in this paper. Two sets of research results are presented. The first set clarifies how a dc drive responds to voltage sags. Voltage sags occur when power systems experience short-circuit faults, which is typically the starting point of dynamic simulation. This research shows that dc drives will trip when they experience relatively large voltage sags. As a result, there is no need to include dc motor drive systems in dynamic studies in this case. Based on the finding, a simple procedure to determine if a dc motor drive system needs to be included for dynamic studies is proposed. The second set of research results presents how to model dc motor drive systems when they experience mild voltage disturbances and are able to ride through. Dynamic models of dc motor drive system dedicated under such conditions are proposed. These models are created by linearizing differential equations of motor drive systems and including the effects of the drive, the motor, and the control system.

In this paper, the overview of load models for power system dynamic studies is provided in Section II. In Section III, the trip-off criteria for dc motor drive systems are provided when the dc drive is subjected to severe voltage sags and will trip (Scenario 1). In Section IV, the dynamic model of dc motor drive systems is proposed when the dc drive is subjected to mild voltage sags and will remain in service without tripping (Scenario 2). The verification of the developed dynamic model is verified through case studies in Section V.

II. Overview of Load Model in Power System Dynamic Studies

The load model is a mathematical representation of the relationship between a bus voltage magnitude and frequency and the active power and reactive power flowing into the bus. The term load model may refer to the equations themselves or the equations plus specific values for the parameters (e.g., coefficients and exponents) of the equations [5]. There are two types of load models: static load models and dynamic load models.

The static load model is a model that expresses the active power and reactive power at any instant of time as functions of the bus voltage magnitude and frequency at the same instant, which involves algebraic equations. Static load models are essentially used for static load components such as resistive and lighting loads. Traditionally, the voltage dependence of load characteristics has been represented by the exponential model [5]

$$P = P_0 \left(\frac{V}{V_0} \right)^a \tag{1}$$

$$Q = Q_0 \left(\frac{V}{V_0} \right)^b . \tag{2}$$

The parameters of this model are the exponents a and b. With these exponents equal to 0, 1, or 2, the model represents

constant power, constant current, or constant impedance characteristics, respectively [5].

An alternative model which has been widely used to represent the voltage dependence of loads is the polynomial model [5]

$$P = P_0 \left[a_1 \left(\frac{V}{V_0} \right)^2 + a_2 \left(\frac{V}{V_0} \right) + a_3 \right] \tag{3}$$

$$Q = Q_0 \left[a_4 \left(\frac{V}{V_0} \right)^2 + a_5 \left(\frac{V}{V_0} \right) + a_6 \right]. \tag{4}$$

This model is also known as "ZIP" model, which consists of the sum of constant impedance (Z), constant current (I), and constant power (P) terms. If the model is used to represent a specific load device, V_0 should be the rated voltage of the device, and P_0 and Q_0 should be the power consumed at rated voltage. However, if the model is used to represent a bus load, V_0, P_0, and Q_0 are normally taken as the values at the initial system operating condition for the study [5]. Polynomials of voltage deviations from rated voltage (ΔV) are sometimes used [5].

The dynamic load model is a model that expresses the active power and reactive power at any instant of time as functions of the voltage magnitude and frequency at a past instant of time and, usually, including the present instant. Difference or differential equations can be used to represent such models [5]. For large industrial loads, two types of dynamic models are proposed in [14]: a transfer function model and an induction motor model with a shunt static load. The dynamic load models are expressed by transfer functions also recommended in [15] and [16]. The transfer function format representing active power and reactive power in dynamic models for power systems is introduced in [15] as follows:

$$\frac{\Delta L(S)}{L_0} = \frac{b_n S^n + \cdots + b_1 S + b_0}{a_n S^n + \cdots + a_1 S + a_0} \frac{\Delta V(S)}{V_0}. \tag{5}$$

Because the transfer function format for dynamic load models has been well accepted, therefore, this load model format is chosen and used for the equivalent dynamic models of dc motor drive systems in this paper.

III. Trip-off Criteria for DC Motor Drive Systems

Power system dynamic studies investigate the system responses after the occurrence of one or multiple disturbances. Typical disturbances are short-circuit faults and subsequent line trips. Such disturbances first appear as voltage sags at various buses of the system. Voltage sags normally do not cause equipment damage but could cause disruption to the operation of sensitive loads. The voltage sag is defined by IEEE standard 1159 as follows: "A decrease to between 0.1 and 0.9 pu in rms voltage at the power frequency for durations of 0.5 cycle to 1 min. Typical values are 0.1 to 0.9 pu." [17]. A voltage sag is characterized by its magnitude and duration. The severity of voltage sag depends on the network structure of the supply system, radial or interconnected for example, and the observation point. The voltage magnitude will depend on the number of phases involved, and the impedance between the observation point and the source of the short circuit. The duration will depend on the speed of the circuit protections, such as fuses, circuit breakers, and differential protections, with a typical clearance time in the range of 100–500 ms [18].

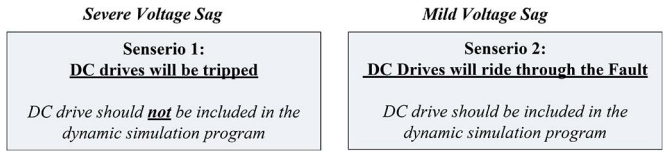

Fig. 1. DC drive operating status subjected to voltage sags.

DC motor drives are particularly susceptible to voltage sags since they normally have no energy storage capacitors [19]. Therefore, it is very important to understand how dc drives respond to voltage sags. Due to their sensitive nature, two scenarios are considered as shown in Fig. 1 when dc drives experience voltage sags. Scenario 1 represents the condition that dc drives will trip when subjected to voltage sags; Scenario 2 represents the condition that dc drives can ride through voltage sags without tripping.

In this paper, to set up trip-off criteria for dc motor drive systems for Scenario 1, the survey on threshold settings of dc drives is conducted, which includes product manuals of industrial dc drives, technical and academic publications, and Electric Power Research Institute (EPRI) field measurement data.

The sensitivity of ASDs to voltage sags is usually expressed as a voltage tolerance characteristic curve in terms of only one pair of parameters, voltage sag magnitude and duration. These two values are denoted as the threshold values. If the voltage sag is longer than the specific duration threshold and deeper than the specific voltage magnitude threshold, the drive will malfunction/trip. In other words, the area below and on the right from the curve represents that voltage sags will cause malfunction/tripping of the drive, while the area above and on the left from the curve represents that voltage sags will not cause the drive tripping [20]–[22]. The voltage tolerance characteristic curve for a drive is determined by overcurrent and undervoltage protections. The undervoltage protection determines the duration threshold, and the overcurrent protection determines the voltage magnitude threshold of the drive sensitivity [20]. As one type of ASDs, the dc drives shall follow the same conventions and be treated as such in this paper.

In [19], it is pointed out that many dc drives are generally set to trip if the voltage magnitude of one, two, or all of the supply phases sags below 90%. DC drives with regenerative bridges are especially sensitive to imbalance and will trip if one phase drops as little as 10% for 1–2 cycles. Most of dc drive manufacturers only indicate the voltage tolerance in terms of depth. For example, For ABB's medium-voltage dc drive (model number DSC 800), voltage tolerance is indicated as −15/+10% [23]. In [24], it is observed that dc drives are very sensitive to voltage drops and will trip when subjected to voltage drops to only 88% of nominal. There may be 5 to 10 trips per year based on the utility average EPRI study. In [25], the field measurement conducted in a newspaper facility in Baltimore is presented. The results are shown in Fig. 2. A sag generator is used to create sags of different depth and duration.

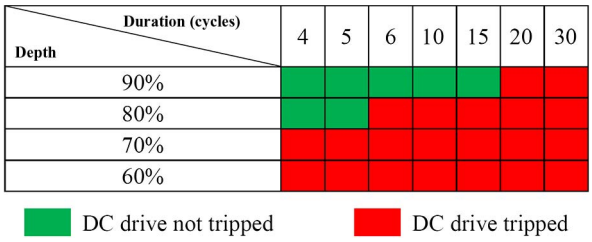

Fig. 2. Response of dc drives to voltage sags [20].

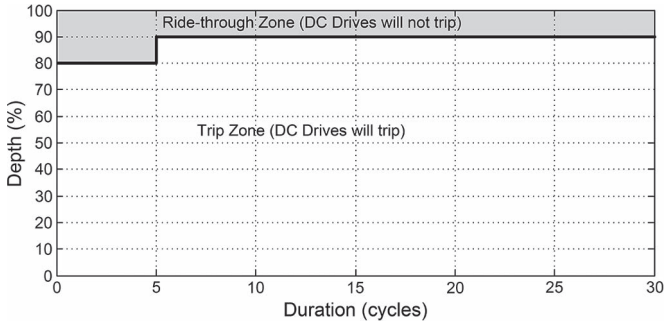

Fig. 3. DC drive trip curve.

In this paper, a dc drive trip curve is proposed based on the survey results as shown in Fig. 3. This curve shows that dc drives will trip for voltage sags below 80% for duration less than 5 cycles (83 ms) or for voltage sags below 90% for duration over 5 cycles (83 ms).

The dc drive trip curve is expressed in terms of the magnitude and duration of voltage sags. If the voltage sag is above the dc drive trip curve, dc drives will not trip and should be included in dynamic studies; if it is below the curve, dc drives will trip and should not be included in dynamic studies.

A simple procedure is proposed to evaluate whether a specific dc drive will trip or not based on the proposed dc drive trip curve.

1) Conduct a three-phase short-circuit study on the study system if the outage event of interest involves a short-circuit fault. In this study, dc drives can be omitted because they only make small contribution to the fault current (for dc drives, the maximum contributing current should be only slightly more than the overload rating of the drive. DC drives contain current limit functions which will interrupt excessive currents in milliseconds [26]). This study will yield a voltage sag magnitude at the dc drive's location.
2) Check the relay setting involved in clearing the fault. This setting will provide the sag duration value for the outage event.
3) The resulting sag magnitude and duration values are then compared with the dc drive trip curve. If the point is below the curve, the dc drives will trip, and they shall not be modeled in dynamic studies. If the point is above the trip curve, the dc drives can ride through the fault. In this case, a detailed dc drive dynamic model is needed for dynamic simulation. Such a dynamic model will be developed and presented in the next section.

IV. Modeling Ride-Through Motor Drive Systems—Equivalent Dynamic Model

For mild voltage disturbances that dc drives are able to ride through, the modeling method of dc motor drive systems is presented in this section. The dynamic model for dc motor drive systems is developed considering the dc drive, the dc motor, and their control system in this research. The developed dynamic model is expressed as an explicit function of system voltage and can be used directly in simulation software in power system dynamic studies.

A. Typical DC Motor Drive and Associated Control System

A typical dc motor drive system consists of a power electronic ac/dc converter and a dc motor in series with a smoothing inductor. For most industrial applications, the power electronic ac/dc converter is a three-phase full-bridge thyristor rectifier as shown in Fig. 4. The configuration of dc drives is based on [13], [27], and [28].

Being mature in theory and practice, the double-loop speed control scheme is the most common method used to adjust the speed of dc motors in industry applications. Fig. 4 shows the schematic diagram of a double-loop speed dc drive control system, which consists of a PI speed controller (ASR) and a PI current controller (ACR). The ASR outputs the armature current reference i_d^* used by the current controller in order to obtain the electromagnetic torque needed to reach the desired speed ω_m^*. The ACR controls the armature current i_d by computing the appropriate thyristor firing angle α, which generates the rectifier output voltage $v_{\rm dc}$ needed to obtain the desired armature current i_d and, thus, the desired electromagnetic torque. Normally, the cosine control of the phase angle (the procedure of "acos") is used to maintain a linear relationship between control signal u_c and the output voltage of the SCR-bridge rectifier $v_{\rm dc}$.

B. Differential Equations for DC Motor Drive Systems

The proposed model is based on the three-phase full-bridge converter dc drive (see Fig. 5), which is widely used for adjustable speed applications in industry. The speed-current double-loop control scheme described in Section IV-A is used in the model. Fig. 6 shows the block diagram detailing the control scheme [28].

The dynamic model of dc motor drive systems is derived from the differential equations representing the dc drive [see (6)–(8)], dc motor [see (9)–(11)], and the control system [see (12) and (13)].

The AVM for dc drives can be expressed as follows:

$$(L_d + 2L_C)\frac{dI_{\rm dc}}{dt} = V_{\rm dc} - E_g - \left(R_d + \frac{3}{\pi}\omega_e L_C\right) I_{\rm dc} \quad (6)$$

where $I_{\rm dc}$ and $V_{\rm dc}$ are the current and voltage at the dc link, E_g is the EMF of the dc motor, ω_e is the fundamental frequency of the power source, R_d and L_d are the dc armature circuit resistance and inductance, respectively, and L_C is the commutating inductance.

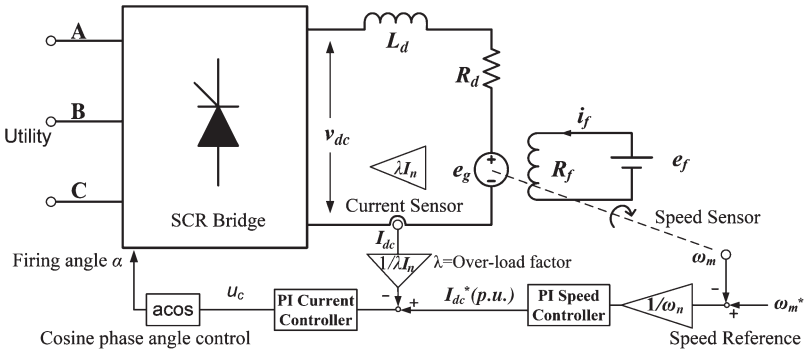

Fig. 4. Schematic diagram of a typical dc motor drive system.

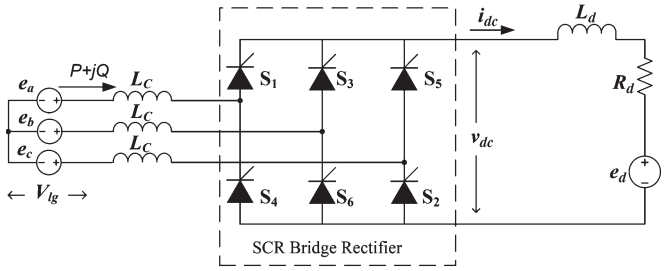

Fig. 5. Three-phase full-converter dc drive (two quadrants) with line commutation.

The commutating inductance (L_C) is the equivalent impedance seen at the input of each drive, which is normally determined by the impedance of the power source, the isolation transformer, the cabling, and other dc drives connected to the same isolation transformer. In practical systems, an isolation transformer may supply more than one dc drives; in this case, the value of L_C for each drive would vary depending on other dc drives and auxiliary loads connected to the same transformer. As a result, with L_C being included, it is hard to make each drive model independent. Therefore, the commutating inductance L_C is excluded from the scope of the model by setting L_C equal to zero. The impact of the commutating inductance is included when aggregating a number of dc drives in the network. The aggregation section is not included in this paper, but it is part of the research work [29].

By neglecting the commutating inductance L_C, (6) is simplified to be

$$L_d \frac{dI_{\rm dc}}{dt} = V_{\rm dc} - E_g - R_d I_{\rm dc}. \tag{7}$$

The average output voltage of the SCR-bridge converter $V_{\rm dc}$ (neglecting commutation inductance L_C) is presented in [11] as follows:

$$V_{\rm dc} = \frac{3\sqrt{6}}{\pi} V_{\rm lg} \cos\alpha \tag{8}$$

where $V_{\rm lg}$ is the utility bus phase-to-ground voltage and α is the firing angle of the SCR bridge.

The mechanical dynamic equation of the dc motor can be expressed as follows:

$$J \frac{d\omega_m}{dt} = T_e - T_m \tag{9}$$

where ω_m is the motor rotating speed, T_e is the electromagnetic torque of the dc motor, T_m is the load torque, and J is the moment of inertia of the dc motor.

The electromagnetic torque T_e can be calculated by

$$T_e = K_T I_{\rm dc} \tag{10}$$

where K_T is the torque constant of the dc motor. The load torque T_m is assumed to be constant.

The relationship between the electromotive force E_g and the rotating speed of the motor ω_m is given as follows:

$$E_g = K_E \omega_m \tag{11}$$

where K_E is the voltage constant of the dc motor $(K_E = K_T)$.

The equation for the PI current controller at the cosine firing angle control mode is

$$\alpha = \arccos\left[-K_{pc}\frac{(I_{\rm dc} - \lambda I_n I_{\rm dc}^*)}{\lambda I_n} - K_{ic}\int_0^t \frac{(I_{\rm dc} - \lambda I_n I_{\rm dc}^*)}{\lambda I_n}\,dt + \cos\alpha_0\right] \tag{12}$$

where K_{pc} and K_{ic} are the proportional and integral gains of the PI current controller, λ is the overloading factor, I_n is the nominal dc-motor armature current, $I_{\rm dc}^*$ is the reference current for the PI current controller, and α_0 is the initial steady-state firing angle of the SCR bridge.

The equation for the PI speed controller can be expressed as follows:

$$I_{\rm dc}^* = \left[-K_{ps}\frac{(\omega_m - \omega_m^*)}{\omega_n} - K_{is}\int_0^t \frac{(\omega_m - \omega_m^*)}{\omega_n}\,dt\right] \tag{13}$$

where ω_n is the nominal speed of the dc motor and K_{ps} and K_{is} are the proportional and integral gains of the PI speed controller.

C. Linearization of Differential Equations

Linearize (7)–(13), and the following are obtained:

$$L_d \frac{d\Delta I_{\rm dc}}{dt} = \Delta V_{\rm dc} - \Delta E_g - R_d \Delta I_{\rm dc} \tag{14}$$

$$J \frac{d\Delta\omega_m}{dt} = K_T \Delta I_{\rm dc} \tag{15}$$

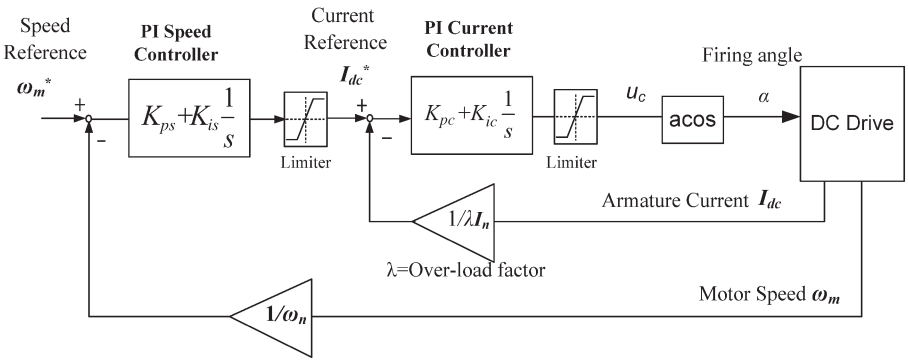

Fig. 6. Control system for the PI speed and current controllers.

$$\Delta E_g = K_E \Delta\omega_m \tag{16}$$

$$\Delta V_{\rm dc} = \frac{V_{\rm dc\,0}}{V_{\rm lg\,0}}\Delta V_{\rm lg} + \frac{3\sqrt{6}}{\pi}V_{\rm lg\,0} \times \left[-K_{pc}\frac{(\Delta I_{\rm dc} - \lambda I_n \Delta I_{\rm dc}^*)}{\lambda I_n} - K_{ic}\int_0^t \frac{(\Delta I_{\rm dc} - \lambda I_n \Delta I_{\rm dc}^*)}{\lambda I_n}\,dt \right] \tag{17}$$

$$\Delta I_{\rm dc}^* = \left(-K_{ps}\frac{\Delta\omega_m}{\omega_n} - K_{is}\int_0^t \frac{\Delta\omega_m}{\omega_n}\,dt \right). \tag{18}$$

Note that the current reference limiter and firing angle limiter are omitted in the linearization process. In fact, it is a common practice to ignore limiters when linearizing dynamic models for power system dynamic studies [30] since the limiters are normally set widely open and would not impact dynamic characteristics under small disturbances.

The Laplace transform is applied to (14)–(18). Substitute (15) in (18), and we have

$$\Delta I_{\rm dc}^* = \left[-\frac{K_{ps}K_T}{J\omega_n}\frac{1}{s}\Delta I_{\rm dc} - \frac{K_{is}K_T}{J\omega_n}\frac{1}{s^2}\Delta I_{\rm dc} \right] \tag{19}$$

where S is the Laplace transform variable.

Substitute (19) in (17), and the following can be obtained:

$$\Delta V_{\rm dc} = \frac{V_{\rm dc\,0}}{V_{\rm lg\,0}}\Delta V_{\rm lg} - \frac{3\sqrt{6}}{\pi}\frac{V_{\rm lg\,0}}{\lambda I_n} \times \left[K_{pc} + \left(K_{ic} + \frac{\lambda K_T I_n K_{pc} K_{ps}}{J\omega_n} \right)\frac{1}{s} + \ldots \frac{\lambda I_n K_T}{J\omega_n}(K_{ic}K_{ps} + K_{pc}K_{is})\frac{1}{s^2} + \frac{\lambda K_T I_n K_{ic} K_{is}}{J\omega_n}\frac{1}{s^3} \right] \Delta I_{\rm dc}. \tag{20}$$

Alternatively, (20) can also be simplified as

$$\Delta V_{\rm dc} = \frac{V_{\rm dc\,0}}{V_{\rm lg\,0}}\Delta V_{\rm lg} - \left[K_{pc} + K_{eq1}\frac{1}{s} + K_{eq2}\frac{1}{s^2} + K_{eq3}\frac{1}{s^3} \right] R_{eq}\Delta I_{\rm dc} \tag{21}$$

where

$$R_{eq} = \frac{3\sqrt{6}}{\pi}\frac{V_{\rm lg\,0}}{\lambda I_n} \tag{22}$$

$$K_{eq1} = K_{ic} + \frac{\lambda K_T I_n K_{pc} K_{ps}}{J\omega_n} \tag{23}$$

$$K_{eq2} = \frac{\lambda I_n K_T}{J\omega_n}(K_{ic}K_{ps} + K_{pc}K_{is}) \tag{24}$$

$$K_{eq3} = \frac{\lambda K_T I_n K_{ic} K_{is}}{J\omega_n}. \tag{25}$$

Substitute (16) in (15), and we have

$$\Delta E_g = \frac{K_E K_T}{J}\frac{1}{s}\Delta I_{\rm dc}. \tag{26}$$

Substitute (21) and (26) in (14), and (27) can be determined.

$$sL_d\Delta I_{\rm dc} + R_d\Delta I_{\rm dc} = \frac{V_{\rm dc\,0}}{V_{\rm lg\,0}}\Delta V_{\rm lg} - \left[K_{pc} + K_{eq1}\frac{1}{s} + K_{eq2}\frac{1}{s^2} + K_{eq3}\frac{1}{s^3} \right] \times R_{eq}\Delta I_{\rm dc} - \frac{K_E K_T}{J}\frac{1}{s}\Delta I_{\rm dc} \tag{27}$$

Reorganizing (27), (28), shown at the bottom of the next page, in the preferred format can be obtained. By substituting (28) in (21), the transfer function of $\Delta V_{\rm dc}$ can be determined in (29) shown at the bottom of the next page.

The relationship between dc-side armature current $I_{\rm dc}$ and ac-side phase current $I_{\rm ac}$ (rms value) can be expressed by

$$I_{\rm ac}(t) = \sqrt{\frac{2}{3}}I_{\rm dc}(t) \tag{30}$$

from the utility side, and the apparent power S, active power P, and reactive power Q consumed by the dc drive can be simply calculated from these dc-side variables

$$S(t) = 3V_{\rm lg}(t)I_{\rm ac}(t) = 3V_{\rm lg}(t)\sqrt{\frac{2}{3}}I_{\rm dc}(t) = \sqrt{6}V_{\rm lg}(t)I_{\rm dc}(t) \tag{31}$$

$$P(t) \approx P_{\rm dc} = V_{\rm dc}(t)I_{\rm dc}(t) \tag{32}$$

$$Q(t) = \sqrt{S(t)^2 - P(t)^2} = I_{\rm dc}(t)\sqrt{6V_{\rm lg}(t)^2 - V_{\rm dc}(t)^2}. \tag{33}$$

Based on (32), the following equation can be obtained:

$$\frac{\Delta P}{\Delta V_{\rm lg}} = \frac{\Delta(V_{\rm dc} I_{\rm dc})}{\Delta V_{\rm lg}} \approx I_{\rm dc\,0} \frac{\Delta V_{\rm dc}}{\Delta V_{\rm lg}} + V_{\rm dc\,0} \frac{\Delta I_{\rm dc}}{\Delta V_{\rm lg}}. \quad (34)$$

For the reactive power Q, (33) can be expanded using multivariable Taylor series at the initial condition as given by

$$\Delta Q = Q - Q_0 \approx \frac{\partial Q}{\partial I_{\rm dc}} \Delta I_{\rm dc} + \frac{\partial Q}{\partial V_{\rm dc}} \Delta V_{\rm dc} + \frac{\partial Q}{\partial V_{\rm lg}} \Delta V_{\rm lg} + \text{high order terms} \ldots . \quad (35)$$

Some approximation is made for (35) by ignoring higher order terms for the three variables, and we have

$$\frac{\Delta Q}{Q_0} = \left(\frac{\Delta I_{\rm dc}}{I_{\rm dc\,0}} - \frac{P_0^2}{Q_0^2} \frac{\Delta V_{\rm dc}}{V_{\rm dc\,0}} \right) + \left[\alpha \frac{\Delta V_{\rm lg}}{V_{\rm lg\,0}} + \beta \left(\frac{\Delta V_{\rm lg}}{V_{\rm lg\,0}} \right)^2 + \gamma \left(\frac{\Delta V_{\rm lg}}{V_{\rm lg\,0}} \right)^3 \right] \quad (36)$$

where

$$\alpha = \frac{S_0^2}{Q_0^2}, \beta = -\frac{0.5 S_0^2}{Q_0^2} \left(\frac{S_0^2}{Q_0^2} - 1 \right), \text{and } \gamma = \frac{0.5 S_0^4}{Q_0^4} \left(\frac{S_0^2}{Q_0^2} - 1 \right).$$

D. Final Equivalent Dynamic Model

Substitute (28) and (29) in (34) and (36), and the final equivalent dynamic model for dc motor drive system can be determined as follows:

$$P = P_0 \left[1 + H(s) \left(\frac{V - V_0}{V_0} \right) \right] \quad (37)$$

$$Q = Q_0 \left[1 + \alpha \left(\frac{V - V_0}{V_0} \right) + \beta \left(\frac{V - V_0}{V_0} \right)^2 + \gamma \left(\frac{V - V_0}{V_0} \right)^3 + D(s) \left(\frac{V - V_0}{V_0} \right) \right]. \quad (38)$$

The input variable of the model is the bus voltage V (line-to-ground) at the locations of the dc drive; the output variables are $P + jQ$. P_0 and Q_0 are the initial steady-state active and reactive power at the drive input, and V_0 is the initial steady-state bus phase-to-ground voltage. $H(s)$ and $D(s)$ are coefficients in the format of fourth-order transfer functions. α, β, and γ are constants. These coefficients are determined by

$$H(s) = \frac{L_d s^4 + \left(\frac{V_{\rm dc\,0}}{I_{\rm dc\,0}} + R_d \right) s^3 + \frac{K_E K_T}{J} s^2}{\left[L_d s^4 + (K_{pc} R_{eq} + R_d) s^3 + \left(K_{eq1} R_{eq} + \frac{K_E K_T}{J} \right) s^2 + K_{eq2} R_{eq} s + K_{eq3} R_{eq} \right]} \quad (39)$$

$$D(s) = \left(-\frac{P_0^2}{Q_0^2} \right) \times \frac{L_d s^4 + \left(R_d - \frac{Q_0^2}{P_0^2} \frac{V_{\rm dc\,0}}{I_{\rm dc\,0}} \right) s^3 + \frac{K_E K_T}{J} s^2}{\left[L_d s^4 + (K_{pc} R_{eq} + R_d) s^3 + \left(K_{eq1} R_{eq} + \frac{K_E K_T}{J} \right) s^2 + K_{eq2} R_{eq} s + K_{eq3} R_{eq} \right]} \quad (40)$$

TABLE I
PARAMETERS OF ELECTRICAL COMPONENTS IN THE SAMPLE DC MOTOR DRIVE SYSTEM (CASE STUDY 1) [28]

Rated Power, HP	40	Load torque TL, N·m	239.36
Nominal Voltage, V	220	Armature Resistance R_d, Ω	0.21
Nominal Current, A	136	Smoothing Inductance L_d, mH	20
Nominal Speed, rpm	1500	Mutual Inductance L_{df}, H	2.621
Motor Inertia, kg·m^2	0.57	Field Current I_f, A	1.5
Controller parameter	PI Speed controller: K_{ps}=10.5, K_{is}=120.5 PI Current controller: K_{pc}=2.48, K_{ic}=37.3 Overload factor λ=1.5		
Initial Steady-state Values	46.0 kW + j27.2 kVar Supply voltage: 208V(L-L) 1500 rpm (full speed)		

TABLE II
PARAMETERS OF THE DEVELOPED DYNAMIC MODEL (CASE STUDY 1)

Parameters	Value
Dynamic Model	Equations (37) and (38)
V_0	1.0
P_0, Q_0	45.90 kW, 27.2 kVar
α, β, γ	[3.849, -5.484, 21.109]
$H(s)$	$\frac{0.015\,s^4 + 1.491 s^3 + 2.785\,s^2}{0.015 s^4 + 3.625\,s^3 + 157.1\,s^2 + 2729 s + 1.78e4}$
$D(s)$	$\frac{0.0427\,s^4 + 0.6828 s^3\,s^2 - 7.936 s^2}{0.015 s^4 + 3.625\,s^3 + 157.1\,s^2 + 2729 s + 1.78e4}$

$$\frac{\Delta I_{\rm dc}}{\Delta V_{\rm lg}} = \frac{I_{\rm dc\,0}}{V_{\rm lg\,0}} \frac{s^3 \frac{V_{\rm dc\,0}}{I_{\rm dc\,0}}}{s^4 L_d + s^3 (K_{pc} R_{eq} + R_d) + s^2 \left(K_{eq1} R_{eq} + \frac{K_E K_T}{J} \right) + s K_{eq2} R_{eq} + K_{eq3} R_{eq}} \quad (28)$$

$$\frac{\Delta V_{\rm dc}}{\Delta V_{\rm lg}} = \frac{V_{\rm dc\,0}}{V_{\rm lg\,0}} \frac{s^4 L_d + s^3 R_d + s^2 \frac{K_E K_T}{J}}{s^4 L_d + s^3 (K_{pc} R_{eq} + R_d) + s^2 \left(K_{eq1} R_{eq} + \frac{K_E K_T}{J} \right) + s K_{eq2} R_{eq} + K_{eq3} R_{eq}} \quad (29)$$

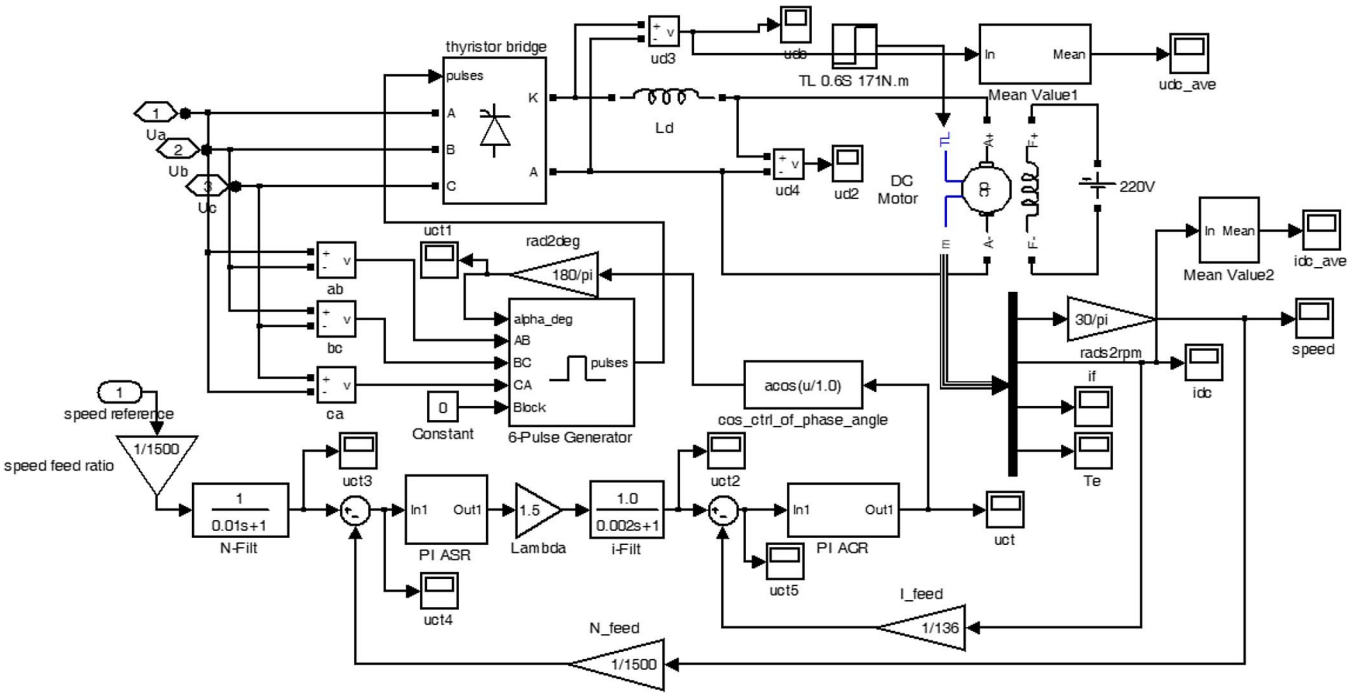

Fig. 7. Detailed switching model simulation circuit for the sample dc motor drive system using Matlab/Simulink (Case Study 1).

$$\alpha = \frac{S_0^2}{Q_0^2}, \quad \beta = -\frac{0.5S_0^2}{Q_0^2}\left(\frac{S_0^2}{Q_0^2} - 1\right), \text{ and}$$

$$\gamma = \frac{0.5S_0^4}{Q_0^4}\left(\frac{S_0^2}{Q_0^2} - 1\right) \tag{41}$$

$$R_{eq} = \frac{3\sqrt{6}}{\pi}\frac{V_{\lg 0}}{\lambda I_n}, \quad K_{eq1} = K_{ic} + \frac{\lambda K_E I_n K_{pc} K_{ps}}{J\omega_n} \tag{42}$$

$$K_{eq2} = \frac{\lambda I_n K_E}{J\omega_n}(K_{ic}K_{ps} + K_{pc}K_{is}),$$

$$K_{eq3} = \frac{\lambda K_E I_n K_{ic} K_{is}}{J\omega_n}. \tag{43}$$

The dc-side state variables for the initial condition can be obtained in [27], [31]

$$I_{\text{dc }0} \approx \sqrt{\frac{3}{2}} I_{\text{ac }0} = \sqrt{\frac{3}{2}}\frac{\sqrt{P_0^2 + Q_0^2}}{3V_{\lg 0}} \tag{44}$$

$$V_{\text{dc }0} = V_{\lg 0} \cdot \frac{3\sqrt{6}}{\pi}\frac{P_0}{\sqrt{P_0^2 + Q_0^2}}. \tag{45}$$

V. Verification of the Developed Dynamic Model

To verify the accuracy of the developed dynamic model, the developed dynamic model was compared against the detailed switching model by two case studies. In the two case studies being created, the dynamic responses of both models subjected to the same system disturbances are simulated and compared. The simulation is conducted using Matlab/Simulink.

A. Case Study 1

The parameters of the sample system [28] for Case Study 1 are given in Table I. The developed equivalent dynamic model for Case Study 1 is shown in Table II.

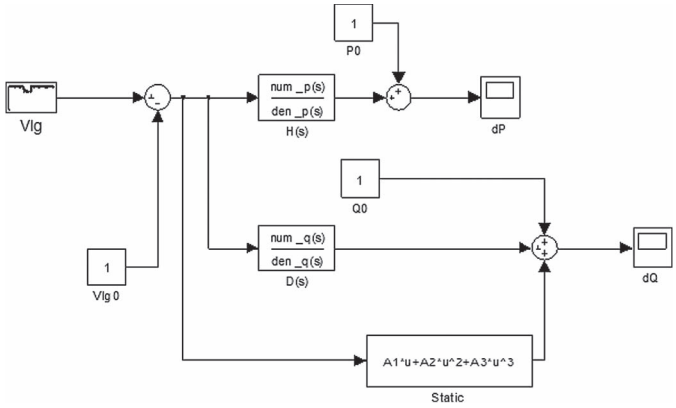

Fig. 8. Developed dynamic model simulation circuit for dc motor drive systems using Matlab/Simulink.

Figs. 7 and 8 show the simulation circuits using Matlab/Simulink for the detailed switching model and the developed dynamic model, respectively.

A three-phase voltage sag with the depth equal to 90% and the duration equal to 0.25 s is applied to the utility power source at the dc drive input at $t = 0.5$ s. Fig. 9 shows the dynamic responses of the developed dynamic model and the detailed switching model subjected to this voltage sag.

B. Case Study 2

The parameters of the sample system [28] for Case Study 2 are given in Table III. The developed equivalent dynamic model for Case Study 2 is shown in Table IV. The simulation circuits for the detailed switching model and the developed dynamic model for Case Study 2 are similar to that of Case Study 1.

A three-phase voltage sag with the depth equal to 85% and the duration equal to 0.25 s is applied to the utility power source

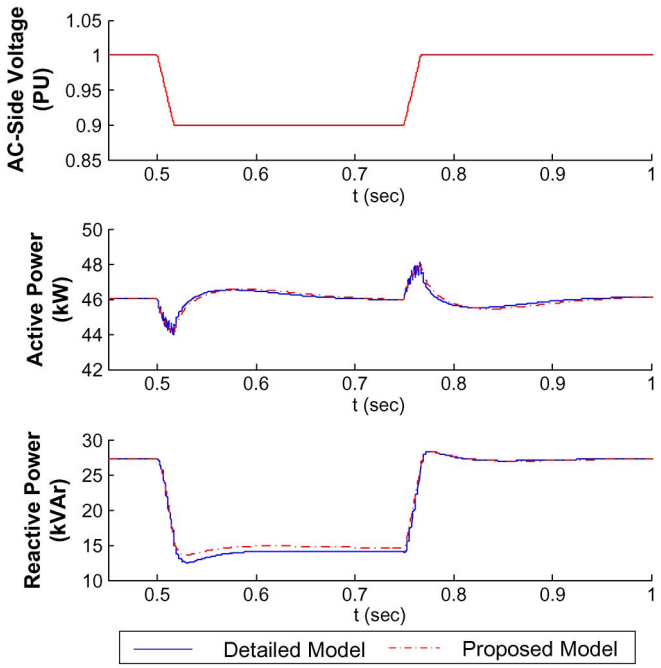

Fig. 9. Dynamic responses of the developed dynamic model and the detailed switching model for 90% voltage sag (Case Study 1).

TABLE III
PARAMETERS OF ELECTRICAL COMPONENTS IN THE SAMPLE DC MOTOR DRIVE SYSTEM (CASE STUDY 2) [28]

Rated Power, HP	120	Load torque TL, N·m	1750
Nominal Voltage, V	220	Armature Resistance R_d, Ω	0.06
Nominal Current, A	462	Smoothing Inductance L_d, mH	4.3
Nominal Speed, rpm	560	Mutual Inductance L_{df}, H	3.59
Motor Inertia, kg·m^2	14.7	Field Current I_f, A	1.5
Controller parameter	PI Speed controller: K_{ps}=118.4, K_{is}=1369 PI Current controller: K_{pc}=1.36, K_{ic}=0.072 Overload factor λ=1.5		
Initial Steady-state Values	107.0kW+j87.4$kVar$, supply voltage: 208V(L-L), 80%full speed		

TABLE IV
PARAMETERS OF THE DEVELOPED DYNAMIC MODEL (CASE STUDY 2)

Parameters	Value
Dynamic Model	Equations (37) and (38)
V_0	1.0
P_0, Q_0	107.0 kW, 87.4 kVar
α, β, γ	[2.534, -1.944, 4.928]
$H(s)$	$\frac{0.005\,s^4+0.474s^3+0.874s^2}{0.005s^4+0.57s^3+208.2s^2+5.08e3s+3.21e4}$
$D(s)$	$\frac{-0.0077\,s^4+0.423s^3-1.341s^2}{0.005s^4+0.57s^3+208.2s^2+5.08e3s+3.21e4}$

at the dc drive input at $t = 0.5$ s. Fig. 10 presents the dynamic responses of the developed dynamic model and the detailed switching model subjected to this voltage sag.

Both case studies (see Figs. 9 and 10) have shown the close match on the dynamic responses between the developed model and the detailed switching model. Note that fast transients are disregarded in the sense since large time steps (i.e., 1/2 cycles) are used in power system dynamic studies.

A slight discrepancy in reactive power may appear. For example, there is an error of reactive power, Q (kVAr), between

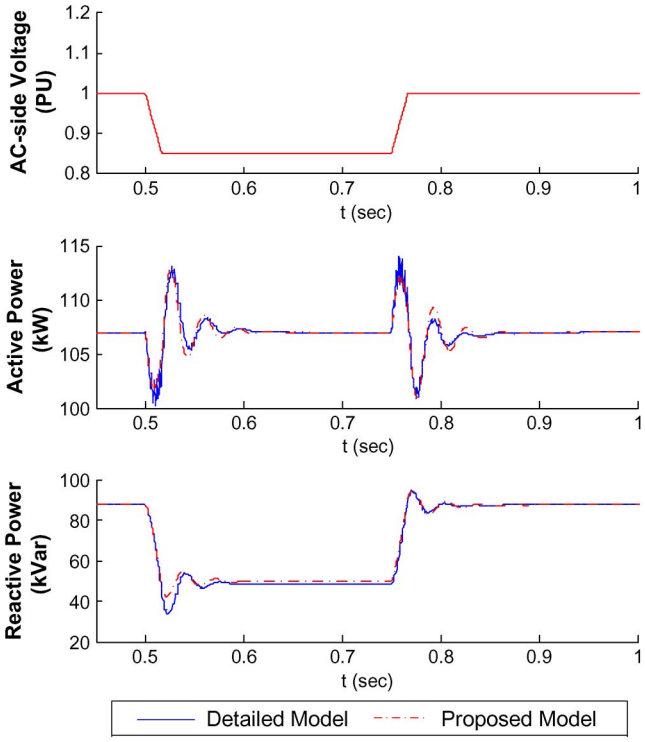

Fig. 10. Dynamic responses of the developed dynamic model and the detailed model for 85% voltage sag (Case Study 2).

0.55 and 0.75 s in Fig. 9. This error was caused by the polynomial approximation introduced in (35). Considering the nature of small disturbances for dc drive ride-through cases, only up to third-order terms are kept, and the higher order terms are discarded. Although keeping the fourth and even higher order terms can achieve higher accuracy, having up to third-order terms appears to be sufficient to maintain a good balance between the accuracy and the model simplicity.

In fact, the steady-state error for active power P (kW) and reactive power Q (kVAr) is always zero at the initial condition. The initial values of the proposed model, (P_0, Q_0), correspond to a given steady-state operating point that the proposed model is linearized from. Therefore, (P_0, Q_0) is intentionally set to the same value observed in the detailed model so that the dynamic response of both models can be equally compared to each other. Note that, in power system dynamic studies, the initial values of the network injection (P_0, Q_0) are specified by the user or given based on the power flow data; other state variables within the dynamic model will be initialized and recalculated based on network injection.

The ringing effect in active power in Fig. 10 is caused by discontinuous and unbalanced ac-side current during the voltage sag, which resulted from rectifier switching. These ripples are in the frequency of 360 Hz, the same as the switching frequency of the full-bridge rectifier. The ripples can be observed in both the developed dynamic model and the detailed switching model.

In summary, the study results show that the proposed equivalent dynamic model can capture the dynamic behavior of the detailed switching model adequately. The accuracy of the

proposed model is deemed to be sufficient for power system dynamic studies.

VI. Conclusion

In this paper, the dynamic modeling of dc motor drive systems has been investigated. The existing work treats dc drives as effectively constant power loads, and there are no dynamic load models available for dc motor drive systems. The contributions of this paper are threefold: 1) it modeled the tripping criterion of dc motor drive systems using a trip curve characterized by fault depth and duration; 2) it developed a complete AVM for the dc motor drive system, including the ac/dc converter, the dc motor, and its associated control system; and 3) it utilized the linearization approach to simplify the complete model as a generic load model format where active and reactive power is given as an explicit function of voltage.

The proposed dynamic model was compared against the detailed switching model in two case studies. The study results show that the proposed model can sufficiently reflect the dynamic response of the detailed switching model with an acceptable degree of approximation.

In comparison to the detailed switching model, the proposed model, based on AVM, is suitable for power system dynamic studies where a large time step is required. Being expressed in generic load model format, the proposed method is readily inserted into commercial simulation software.

The proposed model is deemed to improve the load modeling accuracy for power system dynamic studies such as small-signal stability analysis and transient (large-disturbance) stability analysis. Potential applications include load interconnection studies, distribution planning, and other planning studies that involve the industrial facilities powered by a large portion of dc motor drive loads.

References

[1] K. Sundareswaran and M. Vasu, "Genetic tuning of PI controller for speed control of dc motor drive," in *Proc. IEEE Int. Conf. Ind. Technol.*, 2000, vol. 2, pp. 521–525.
[2] G. Kulak, E. Nowicki, and W. Rosehart, "Engineering considerations when replacing an old dc drive system," in *Proc. IEEE Power Eng. Soc. Summer Meet.*, 2002, vol. 2, pp. 664–668.
[3] A. T. Alexandridis and D. P. Iracleous, "Optimal nonlinear firing angle control of converter-fed dc drive systems," in *Proc. Inst. Elect. Eng.–Elect. Power Appl.*, May 1998, vol. 145, no. 3, pp. 217–222.
[4] T. G. Martinich and J. B. Neilson, "Mitigation of resonance using digital models and direct measurement of harmonic impedances," in *Proc. IEEE Power Eng. Soc. Summer Meet.*, 2000, vol. 2, pp. 1069–1074.
[5] "Load representation for dynamic performance analysis," *IEEE Trans. Power Syst.*, vol. 8, no. 2, pp. 472–482, May 1993.
[6] "Standard load models for power flow and dynamic performance simulation," *IEEE Trans. Power Syst.*, vol. 10, no. 3, pp. 1302–1313, Aug. 1995.
[7] G. Shahgholian and P. Shafaghi, "State space modeling and eigenvalue analysis of the permanent magnet dc motor drive system," in *Proc. ICECT*, May 7–10, 2010, pp. 63–67.
[8] H. Qian, D. Grignion, X. Chen, and N. Kar, "Discrete time robust load disturbance torque estimator for a dc motor drive system," in *Proc. IEEE Int. CCA*, Oct. 3–5, 2012, pp. 86–91.
[9] *ETAP User Guide*, OTI Inc., Ottawa, ON, Canada, 2012.
[10] A. Merdassi, L. Gerbaud, and S. Bacha, "A new automatic average modelling tool for power electronics systems," in *Proc. IEEE PESC*, 2008, pp. 3425–3431.
[11] J. Sun and H. Grotstollen, "Averaged modeling of switching power converters: Reformulation and theoretical basis," in *Proc. 23rd Annu. IEEE PESC*, 1992, vol. 2, pp. 1165–1172.
[12] S. Cuk and R. D. Middlebrook, "A general unified approach to modelling switching-power-stages," in *Proc. IEEE PESC*, 1976, pp. 18–31.
[13] P. C. Krause, O. Wasynczuk, and S. D. Sudhoff, *Analysis of Electric Machinery and Drive Systems*, 2nd ed. Piscataway, NJ, USA: IEEE Press, 2002.
[14] S. A. Y. Sabir and D. C. Lee, "Dynamic load models derived from data acquired during system transients," *IEEE Trans. Power App. Syst.*, vol. PAS-101, no. 9, pp. 3365–3372, Sep. 1982.
[15] T. Omata and K. Uemura, "Effects of series impedance on power system load dynamics," *IEEE Trans. Power Syst.*, vol. 14, no. 3, pp. 1070–1077, Aug. 1999.
[16] F. T. Dai, J. V. Milanovic, N. Jenkins, and V. Roberts, "Development of a dynamic power system load model," in *Proc. 7th IEE Int. Conf. AC-DC Power Transmiss.*, Nov. 28–30, 2001, pp. 344–349.
[17] *IEEE Recommended Practice for Monitoring Electric Power Quality*, IEEE Standard 1159, 1995.
[18] A. Sudria *et al.*, "Grid voltage sags effects on frequency converter drives and controlled rectifier drives," in *Proc. IEEE Compat. Power Electron.*, 2005, pp. 39–45.
[19] N. S. Tunaboylu, E. R. Collins, Jr., and S. W. Middlekauff, "Ride-through issues for dc motor drives during voltage sags," in *Proc. IEEE Southestcon, Vis. Future*, 1995, pp. 52–58.
[20] S. Z. Djokic, K. Stockman, J. V. Milanovic, J. J. M. Desmet, and R. Belmans, "Sensitivity of ac adjustable speed drives to voltage sags and short interruptions," *IEEE Trans. Power Del.*, vol. 20, no. 1, pp. 494–505, Jan. 2005.
[21] S. Z. Djokic, S. M. Munshi, and C. E. Cresswell, "The influence of overcurrent and undervoltage protection settings on ASD sensitivity to voltage sags and short interruptions," in *Proc. 4th IET Conf.PEMD*, 2008, pp. 130–134.
[22] X. Liang and W. Xu, "Modeling variable frequency drives and motor systems in power systems dynamic studies," in *Conf. Rec. IEEE IAS Annu. Meeting*, Orlando, FL, USA, Oct. 6–11, 2013, pp. 1–11.
[23] *ABB Product Guide, Standard DC Drives DSC 550*, ABB Inc., Cary, NC, USA, 2012.
[24] J. Lamoree, D. Mueller, P. Vinett, and W. Jones, "Voltage sag analysis case studies," *IEEE Trans. Ind. Appl.*, vol. 30, no. 4, pp. 1083–1089, Jul./Aug. 1994.
[25] Electric Power Research Institute (EPRI), "Printing Press Shutdowns Caused By Sensitivity of DC Drive to Voltage Sags," Electric Power Res. Inst., Knoxville, TN, USA, 2000.
[26] Rockwell Automation, at 1:40 am. "Adjustable speed drives and short circuit currents," Jun. 13, 2014 at 1:40 am. [Online]. Available: http://www.ab.com/support/abdrives/documentation/ techpapers/afdscc.htm
[27] P. C. Sen, *Thyristor DC Drives*. Hoboken, NJ, USA: Wiley, 1981.
[28] S. Zhang, (in Chinese), , *DC Converter Electric Drive System*., 2nd ed. Wuhan, China: Huazhong Univ. Science Technol. Press, 1995.
[29] S. Li, "Load Modeling Techniques for Power System Dynamic Studies," M.S. thesis, Univ. Alberta, Edmonton, AB, Canada, 2013.
[30] P. Kundur, *Power System Stability and Control*. Englewood Cliffs, NJ, USA: McGraw-Hill, 1994.
[31] W. Xu, H. W. Dommel, M. Brent Hughes, and Y. Liu, "Modelling of dc drives for power system harmonic analysis," *Proc. Inst. Elect. Eng.–Gener. Transmiss. Distrib.*, vol. 146, no. 3, pp. 217–222, May 1999.

Shengqiang Li (S'12–M'13) received the B.Eng. degree in electrical engineering from Zhejiang University, Hangzhou, China, and the M.Sc. degree in electrical and computer engineering from the University of Alberta, Edmonton, AB, Canada.

He is currently with Powertech Labs Inc., Surrey, BC, Canada, as a Power System Studies Engineer. His research interests include power system modeling and stability studies.

Xiaodong Liang (M'06–SM'09) was born in Lingyuan, China. She received the B.Eng. and M.Eng. degrees in electrical engineering from Shenyang Polytechnic University, Shenyang, China, in 1992 and 1995, respectively, the M.Sc. degree in electrical engineering from the University of Saskatchewan, Saskatoon, SK, Canada, in 2004, and the Ph.D. degree in electrical engineering from the University of Alberta, Edmonton, AB, Canada, in 2013.

From 1995 to 1999, she served as a Lecturer in the Department of Electrical Engineering, Northeastern University, Shenyang, China. In October 2001, she joined Schlumberger in Edmonton, AB, Canada. She was a Principal Power Systems Engineer with Schlumberger before she joined Washington State University, Vancouver, WA, USA, as an Assistant Professor in August 2013. Her research interests include power system dynamics, power quality, and electric machines.

Dr. Liang is a Registered Professional Engineer in the Province of Alberta, Canada.

Wilsun Xu (M'90–SM'95–F'05) received the Ph.D. degree from the University of British Columbia, Vancouver, BC, Canada, in 1989.

He was an Engineer with BC Hydro, Burnaby, BC, Canada, from 1990 to 1996. He is currently a Professor and NSERC/iCORE Industrial Research Chair at the University of Alberta, Edmonton, AB, Canada. His research interests are power quality and power system modeling.